Alloying dichalcogenolate-protected Ag-21 eight-electron nanoclusters: a DFT investigation

Franck Gam, Isaac Chantrenne, Samia Kahlal, Tzu-Hao Chiu, Jian-Hong Liao, C. W. Liu, Jean-Yves Saillard

Alloying dichalcogenolate-protected Ag_{21} 8-electron nanoclusters: A DFT investigation

Franck Gam,[a] Isaac Chantrenne,[a] Samia Kahlal,* [a] Tzu-Hao Chiu,[b] Jian-Hong Liao,[b] C. W. Liu * [b] and Jean-Yves Saillard *[a]

The isoelectronic doping of dichalcogenolato nanoclusters of the type $[Ag_{21}\{E_2P(OR)_2\}_{12}]^+$ (E = S, Se) by any heteroatom belonging to groups 9-12 is systematically investigated by DFT calculations. Although they can differ in their global structure, all these species have the same $M@M_{12}$ centered icosahedral core. In any case, the different structure-types are found to be very close in energy. In all of them, three different alloying sites can be identified (central, icosahedral, peripheral) and calculations allow revealing the trends in the heteroatom site occupation preference across the group 9-12 family. These trends are supported by complementary experimental results. They are rationalized on the basis of electronegativity, potential involvement in the bonding of valence d-orbitals and atom size. TD-DFT calculations show that the effect of doping on the optical properties is sizable and therefore should stimulate experimentalists interested in modulating luminescence properties, both in the dithiolato and diseleno families of complexes.

Introduction

During the last decades, ligand-protected atom-precise noble metal nanoclusters have remained the subject of an immense scientific interest, due to their stunning structural and bonding features, as well as their numerous chemical and physicochemical properties.[1-25] A way of tuning the properties of an homometallic nanocluster is to "alloy" it by substituting one or several metal atoms with another metal from the same or a nearby column.[18,19] Fine control of properties upon alloying necessitates controlling the number and position(s) of the heterometal atom(s) in the nanocluster molecular framework. This is not always an easy task to realize experimentally, owing to the difficulties inherent to alloy characterization, such as separation of alloys of different compositions and/or of positional isomers, as well as crystal disorder. This is why density functional theory (DFT) modelization has been used as a complementary tool to help determining precise structure of alloys, and rationalizing their stabilities, peculiar electronic features and structure/properties relationships.[6,25-40] So far, most of these theoretical investigations were devoted to thiolate-protected alloys of gold, or to a limited number of their silver-equivalent alloyed homologues. With respect to silver alloys, the most comprehensive theoretical investigation was made by Aikens and coworkers on the doping of $[Ag_{25}(SR)_{18}]^-$, who found that group 10 atoms prefer central location, whereas the other positions become more preferable when doping with group 11-13 atoms.[39] During the last years, some of us developed an original chemistry of silver nanoclusters protected by dichalcogenolate ligands of general formula $[Ag_{21}\{E_2P(OR)_2\}_{12}]^+$.[41,42] (E = S, Se). Their originality comes from the distinctive nature of the dichalcogenolate ligands which differ from simple thiolates not only by their chelating nature but also by the fact they bear a different formal charge per coordinating atom (-1 for *two* chalcogens *vs.* -1 for *one* sulfur in the case of thiolates). As a result, dichalcogenolates stabilize species with nuclearities and compositions that are noticeably different from that of simple thiolates. Such compounds have no equivalent within gold nanocluster chemistry and their diseleno derivatives are the only examples of isolated Se-protected silver nanoclusters structurally characterized so far. They consist of a *superatomic* $[Ag_{13}]^{5+}$ centered icosahedral core, protected by an outer passivating shell made of 12 dichalcogenolate ligands and 8 Ag(I) outer d^{10} metals. Isoelectronic alloys have also been already characterized, namely $[\{Au@Ag_{20}\}\{Se_2P(OEt)_2\}_{12}]^+$,[41] $[\{Pt@Ag_{20}\}\{S_2P(O^nPr)_2\}_{12}]$,[43] $[\{Pt@Ag_{20}\}\{Se_2P(O^nPr)_2\}_{12}]$,[44] $[\{Pt@Ag_{20}\}\{Se_2P(O^iPr)_2\}_{12}]$,[44] $[\{Pt@Ag_{20}\}\{Se_2P(CH_2CH_2Ph)_2\}_{12}]$,[44] $[\{Pd@Ag_{20}\}\{S_2P(O^nPr)_2\}_{12}]$,[45] $[\{Au@Ag_{20}\}\{S_2P(O^iPr)_2\}_{12}]^+$,[46] $[Au@Ag_{20}\}\{Se_2P(O^iPr)_2\}_{12}]^+$,[47] $[\{Au@Au_2Ag_{18}\}\{Se_2P(O^iPr)_2\}_{12}]^+$,[47] $[\{Ag@Ag_{16}Cu_4\}\{S_2P(O^iPr)_2\}_{12}]^+$ [48] and $[\{Au@Ag_{16}Cu_4\}\{S_2P(O^iPr)_2\}_{12}]$.[48]

Three structural types have been clearly shown to exist so far within this rather large family of homo- and heterometallic compounds (Figure 1), all of them having the same M_{13} centered icosahedral *superatomic* core,

but differing by the topology of their outer passivating shell made of 12 dichalcogenolate ligands and 8 d^{10} outer metals (Figure 2), which are distinctly different from the family of the $[MAu_{24}(SR)_{18}]^-$ and $[MAg_{24}(SR)_{18}]^-$ monothiolato alloys.[39] In this paper, we present a systematic and comprehensive theoretical investigation on the stability, structure and optical properties of such silver nanoclusters isoelectronically monosubstituted by a metal of group 9 (Co, Rh, Ir), 10 (Ni, Pd, Pt), 11 (Cu, Au) or 12 (Zn, Cd, Hg), together with some experimental X-ray and UV-vis results that support the computed results. All the investigated species are isoelectronic to their $[Ag_{21}\{E_2P(OR)_2\}_{12}]^+$ parent, *i.e.* are 8-electron *superatoms*[1,2,13,23, 42,49,50] of configuration $1S^2\ 1P^6$.

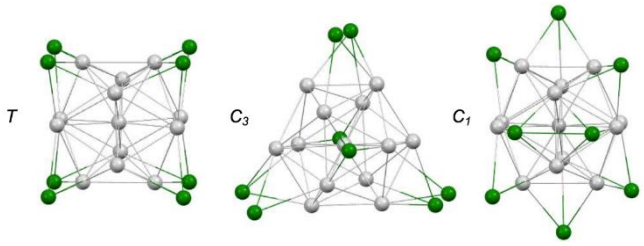

Figure 1. Structurally characterized 8-electron $[Ag_{21}\{E_2P(OR)_2\}_{12}]^+$ (E = S, Se) clusters and their isoelectronic alloys. The ideal symmetries are those of the whole cluster, assuming that all the metal atoms are of the same nature.

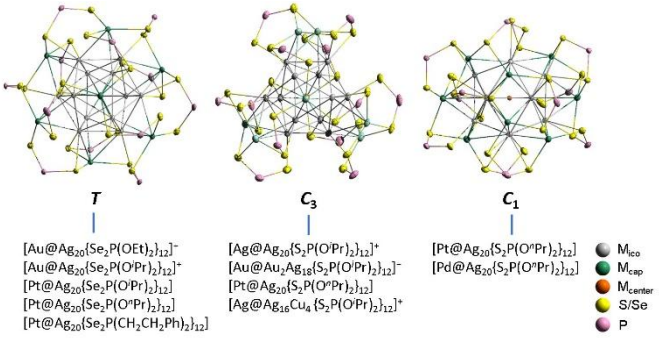

Figure 2. The octa-capped centered icosahedral metal frameworks ($[M@M_{12}][\mu_3\text{-}M_8]$) of the three structural types defined in Fig. 1. They differ only by the position of the eight face-capping outer d^{10} (*eg*. Ag(I)) atoms (in green). The positions of the twelve ligands (Fig. 1) ensue from that of these eight atoms. The specified *T*, C_3 and C_1 symmetries are that of the whole cluster (with ligands), considered as homometallic. They correspond to the T_h, D_3 and C_2 ideal symmetries for the naked M_{21} framework, respectively (see Fig. 1).

Computational details

DFT calculations were carried out with the Gaussian 16 package[52] on the various isomers of models $[MAg_{20}(E_2PH_2)_{12}]^q$ (E = S, Se; M = Co, Rh, Ir: q = -1; M = Ni, Pd, Pt: q = 0; M = Cu, Ag, Au: q = +1; M = Zn, Cd, Hg: q = +2). The considered ligand simplification allows to save a huge amount of CPU time. On the other hand, its validity has been proven in many occasions.[41-48,52] The BP86 functional[53,54] was used together with the general triple-ζ polarized Def2-TZVP basis set from EMSL Basis Set Exchange Library,[55,56] in conjunction with effective core potentials (ECP's) for the eight heavier elements, thus permitting to somewhat account for scalar relativistic effects. All the optimized geometries were ascertained as true minima on the potential energy surface by carrying out vibrational frequency calculations. All the investigated species were found to have a singlet ground state. The natural atomic orbital (NAO) charges were computed with the NBO 6.0 program on single-point calculations at the same level of theory.[57] The UV-visible transitions were calculated on the above-mentioned optimized geometries by means of time-dependent DFT (TD-DFT) calculations, with the CAM-B3LYP functional[58] and the

Def2-TZVP basis set. The UV-visible spectra were simulated from the computed TD-DFT transitions and their oscillator strengths by using GaussView,[59] each transition being associated with a Gaussian function of half-height width equal to 1000 cm^{-1}.

Experimental details

The synthesis of $[PtAg_{20}\{S_2P(O^nPr)_2\}_{12}]$ was performed according to previous report.[43] Whereas crystals containing the C_1-*I* isomer ($P2_1/c$ space group) were obtained by diffusing *n*-hexane into dichloromethane solution at ambient temperature and contain solvated *n*-hexane molecules,[43] those of the C_3-*I* isomer (*R*3 space group) were grown in acetone at ambient temperature. A single crystal suitable for X-ray diffraction analysis was mounted on the tip of glass fiber coated in paratone oil, then frozen. Data were collected on a Bruker APEX II CCD diffractometer using graphite monochromated Mo Kα radiation (λ = 0.71073 Å) at 100 K. Absorption corrections for area detector were performed with SADAB[60] and the integration of raw data frame was performed with SAINT.[61] The structure was solved by direct methods and refined by least-squares against F^2 using the SHELXL-2018/3 package,[62,63] incorporated in SHELXTL/PC V6.14.[64] All non-hydrogen atoms were refined anisotropically. One of the propyl groups (C10-C12) was found disordered over two positions with equal occupancy. Crystallographic data are provided in Table S1. The structure reported herein has been deposited at the Cambridge Crystallographic Data Centre, CCDC no. 2091674. UV-visible absorption spectra were measured on a Perkin Elmer Lambda 750 spectrophotometer using quartz cells with path length of 1 cm. All samples were recorded at ambient temperature in 2-MeTHF as solvent.

Energetic and structural results

As said above, the three different structures so far characterized are strongly related.[65.] Not only they all possess a formally 8-electron centered icosahedral M_{13} core, but in all of them the 12 dichalcogenolate ligands are arranged in such a way that the 12

metal atoms occupying icosahedral vertices are coordinated to one sulfur/selenium atom in a radial orientation and the 8 peripheral outer d^{10} centers are coordinated in a trigonal planar mode, making thus locally stable 16-electron complexes. These d^{10} metals are capping icosahedral faces, but their interaction with the icosahedral core is weak[41-48,52] (mainly of metallophilic nature). Assuming a homometallic $[Ag_{21}\{E_2P(OR)_2\}_{12}]^+$ cluster in any of the three structures defined above, the substitution of any of the Ag atoms by one hetero-metal generates several positional isomers to calculate, the number of which becoming very large in the case of the structure of C_1 symmetry. In order to reduce the number of structures to calculate, we have first computed the homometallic $[Ag_{21}\{E_2PH_2\}_{12}]^+$ (E = S, Se) in the three characterized structural types shown in Figures 1 and 2. We thus assume that the role played by the nature of R in the structural choice of the $[Ag_{21}\{E_2P(OR)_2\}_{12}]^+$ (E = S, Se) clusters and their alloys is negligible. This is, *inter alia*, supported by the fact that all the known diselenolato species adopt the same structure-type *T*, independently from the size and nature of R (Figure 1). Selected computed results are given in Table 1. The dithiolato species have their free energies lying in a range of less than 5 kcal/mol, whereas that of their diselenolato relatives range within less than 11 kcal/mol. In both cases, the C_1 structure is the less stable. All the computed structures have related electronic structures, as exemplified by the nature of their HOMOs and LUMOs,[41] HOMO-LUMO gaps and the NAO charges of the different types of Ag atoms (icosahedron center (Type I), icosahedron vertices (Type II) and outer capping Ag(I) centers (Type III)). Owing to the similarities

of the computed results for the three structures and their closeness in energy, we chose to focus on the two more stable and more symmetrical ones, namely *T* and C_3.

Table 1. Selected results obtained for the $[Ag_{21}\{E_2PH_2\}_{12}]^+$ (E = S, Se) models in the three experimentally characterized structural types discussed in the text. HOMO-LUMO gaps (H-L) in eV and relative total (ΔE) and free (ΔG) energies in kcal/mol.

Cluster	Symmetry	H-L	ΔE	ΔG	NAO charges
$[Ag_{21}\{S_2(PH_2)\}_{12}]^+$	*T*	1.92	0.1	2.1	center: -0.37 icosahedron: +0.23 outer capping: +0.63 (+0.61; +0.64)
	C_3	1.77	0	0	center: -0.41 icosahedron: +0.23 (+0.21; +0.25) outer capping: +0.63 (+0.60; +0.64)
	C_1	1.45	8.6	4.6	center: -0.42 icosahedron: +0.23 (+0.07; 0.30) outer capping: +0.63 (+0.61; +0.65)
$[Ag_{21}\{Se_2(PH_2)\}_{12}]^+$	*T*	1.73	0	0	center: -0.29 icosahedron: +0.21 outer capping: +0.58 (+0.56; +0.60)
	C_3	1.52	4.6	0.2	center: -0.34 icosahedron: +0.21 (+0.18; 0.23) outer capping: +0.58 (+0.55; +0.59)
	C_1	1.29	15.6	10.3	center: -0.34 icosahedron: +0.20 (+0.06; +0.29) outer capping: +0.58 (+0.57; 0.60)

Substituting one of the Ag atoms in $[Ag_{21}(E_2PH_2)_{12}]^+$ by an hetero-metal M generates four and seven different $[MAg_{20}(E_2PH_2)_{12}]^q$ positional isomers for the *T* and C_3 structures, respectively, as illustrated in Figure 3. Note that, because of the substitution, most of these isomeric structures have a symmetry lower than that of their *T* or C_3 $[Ag_{21}(E_2PH_2)_{12}]^+$ progenitor. Thus, in the followings, the *T* and C_3 labels will designate a structure type, rather than a symmetry group.

The relative energies and HOMO-LUMO gaps of the most stable isomers of the $[MAg_{20}(E_2PH_2)_{12}]^q$ systems derived from structure types *T* and C_3 are given in Table 2. More detailed energetical results concerning all the isomers defined in Figure 3 are provided in Tables S2 and S3. Starting with the thiolato (E = S) series, one can see that the C_3 structure type is always preferred over the *T* one, both in ΔE and ΔG, but in any case by less than □6 kcal/mol. These results are in line with those obtained for the homometallic $[Ag_{21}\{S_2PH_2\}_{12}]^+$ cluster (see above). Moreover, except for M = Cd, the preferred substitution site (I, II or III) is the same for the *T* and C_3 structures. When M belong to groups 9 and 10, there is a neat preference for type I, *i.e.*, for M occupying the icosahedron center. This result is consistent with the X-ray structures of $[\{Pt@Ag_{20}\}\{S_2P(O^nPr)_2\}_{12}]$ [43] and $[\{Pd@Ag_{20}\}\{S_2P(O^nPr)_2\}_{12}]$,[45] This preference for type I is stronger for group 9 that for group 10 metals and within each group, it is increasing when descending the triad (Table S2). Type I is also clearly preferred for M = Au and this is corroborated by the X-ray structure of $[\{Au@Ag_{20}\}\{S_2P(O^iPr)_2\}_{12}]^+$.[46] However, this preference is somewhat less important than for M = Pt. With M = Cu, type III, *i.e.*, Cu occupying an outer capping position, is preferred. This is also the case of M = Zn. In the case of M = Cd, Types III and II are almost isoenergetic, whereas for M = Hg, type II, *i.e.*, Hg occupying an icosahedron vertex, is preferred.

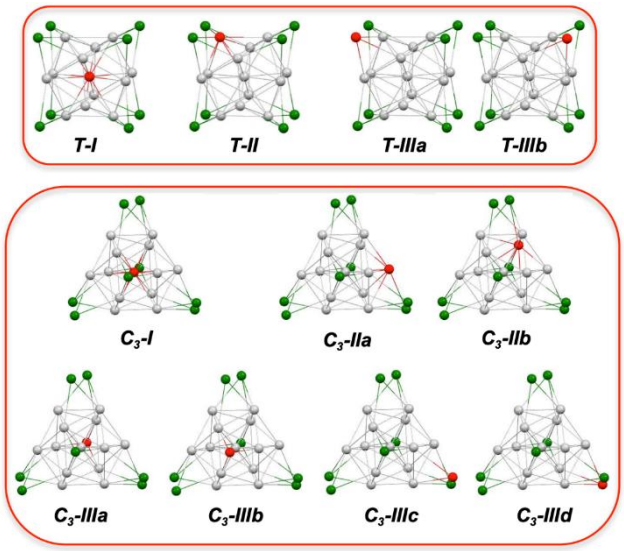

Figure 3. The different isomers generated by substituting one Ag atom by one hetero-metal M in the *T* and C_3 structure types of $[Ag_{21}\{E_2P(OR)_2\}]^+$. Color code: Ag, grey (centered icosahedron), green (outer capping); M; red. Ligand not shown.

The selenolato (E = Se) series exhibits quite similar trends, with some small differences. In particular, the energy differences between structure-type *T* and C_3 are even smaller than in the E = S case and *T* is slightly preferred over C_3 in ΔE, whereas the opposite situation occurs in ΔG. One can simply note that all the $[MAg_{20}(Se_2PH_2)_{12}]^q$ X-ray structures determined so far adopt the *T* structure-type. The other slight differences with the thiolato series concerns the M = group 12 cases for which the energy differences between positional isomers are small. Zn balances between type II and type I and Cd and Hg slightly prefer type II. The so far known experimental structures of $[MAg_{20}(Se_2PH_2)_{12}]^q$ species, namely that of $[\{Pt@Ag_{20}\}\{Se_2P(O^nPr)_2\}_{12}]$,[45] $[\{Au@Ag_{20}\}\{Se_2P(OEt)_2\}_{12}]^+$ [42] and $[Au@Ag_{20}\}\{Se_2P(O^iPr)_2\}_{12}]^+$ [47] support our computed results.

Finally, we would like to bring additional support to the fact that the C_1 structure was not considered in the above calculations on alloys, based on the fact the three structural types of Figure 1 are very close in energy, independently from the nature of M, and do not impact on the positional choice of M on the alloy metal framework (I, II or III). It turns out that we just characterized the C_3 structure of $[\{Pt@Ag_{20}\}\{Se_2P(O^nPr)_2\}_{12}]$, whereas the C_1 structure of the same compound is already known (Figure 1).[43] This is actually the first example of true isomerism (same R substituent) reported in the chemistry of silver or silver-rich nanoclusters. Both isomers are of type I, as predicted by the calculations. They were obtained from different crystallization conditions (see Experimental details). This new C_3-*I* X-ray structure is shown in Figure 4 and has comparable metrical data to its C_1-*I* isomer (see SI for more details). Calculations on the C_3-*I* and C_1-*I* isomers of the $[PtAg_{20}(E_2PH_2)_{12}]$ model found an energy difference of 5.6 kcal/mol (C_3-*I* more stable). This existence of true isomers underpins also the negligible role played by the nature of the R substituent on the preference for one of the structures of Figure 1 over the others.

		E = Se							
		T				C_3			
		Isomer	H-L	ΔE	ΔG	Isomer	H-L	ΔE	ΔG
group 9	$[CoAg_{20}(L)_{12}]^-$	*T-I*	1.75	0.0	2.0	C_3-*I*	1.53	0.7	0.0
	$[RhAg_{20}(L)_{12}]^-$	*T-I*	1.36	0.0	2.0	C_3-*I*	1.23	0.7	0.0
	$[IrAg_{20}(L)_{12}]^-$	*T-I*	1.86	0.0	2.5	C_3-*I*	1.62	0.1	0.0
group 10	$[NiAg_{20}(L)_{12}]$	*T-I*	1.69	0.0	0.9	C_3-*I*	1.51	3.1	0.0
	$[PdAg_{20}(L)_{12}]$	*T-I*	1.73	0.0	0.7	C_3-*I*	1.54	3.3	0.0
	$[PtAg_{20}(L)_{12}]$	*T-I*	1.83	0.0	0.8	C_3-*I*	1.62	2.9	0.0
group 11	$[CuAg_{20}(L)_{12}]^+$	*T-IIId*	1.70	0.0	0.0	C_3-*IIIb*	1.53	2.6	1.2
	$[AuAg_{20}(L)_{12}]^+$	*T-I*	1.83	0.0	0.1	C_3-*I*	1.59	4.3	0.0
group 12	$[ZnAg_{20}(L)_{12}]^{2+}$	*T-I*	1.78	0.0	2.3	C_3-*IIa*	1.35	0.4	0.0
	$[CdAg_{20}(L)_{12}]^{2+}$	*T-II*	1.61	0.0	0.0	C_3-*IIIa*	1.27	3.1	1.0
	$[HgAg_{20}(L)_{12}]^{2+}$	*T-II*	1.45	0.0	5.3	C_3-*IIb*	1.42	3.4	0.0

Table 2. Computed HOMO-LUMO gaps (H-L) (in eV) and relative total (ΔE) and free (ΔG) energies (in kcal/mol) of the most stable isomers of clusters $[MAg_{20}(L)_{12}]^q$ (L = E_2PH_2) found for structure types *T* and C_3, as defined in Fig. 3.

		E = S							
		T				C_3			
		Isomer	H-L	ΔE	ΔG	Isomer	H-L	ΔE	ΔG
group 9	$[CoAg_{20}(L)_{12}]^-$	*T-I*	1.46	3.3	4.7	C_3-*I*	1.36	0.0	0.0
	$[RhAg_{20}(L)_{12}]^-$	*T-I*	1.91	2.8	5.4	C_3-*I*	1.73	0.0	0.0
	$[IrAg_{20}(L)_{12}]^-$	*T-I*	2.04	4.2	6.0	C_3-*I*	1.84	0.0	0.0
group 10	$[NiAg_{20}(L)_{12}]$	*T-I*	1.82	1.4	4.1	C_3-*I*	1.72	0.0	0.0
	$[PdAg_{20}(L)_{12}]$	*T-I*	1.92	1.0	3.6	C_3-*I*	1.81	0.0	0.0
	$[PtAg_{20}(L)_{12}]$	*T-I*	2.04	1.8	4.3	C_3-*I*	1.91	0.0	0.0
group 11	$[CuAg_{20}(L)_{12}]^+$	*T-IIIa*	1.90	4.7	1.6	C_3-*IIIc*	1.75	0.0	0.0
	$[AuAg_{20}(L)_{12}]^+$	*T-I*	2.03	0.4	2.1	C_3-*I*	1.87	0.0	0.0
group 12	$[ZnAg_{20}(L)_{12}]^{2+}$	*T-IIIb*	1.69	5.8	6.4	C_3-*IIIa*	1.50	0.0	0.0
	$[CdAg_{20}(L)_{12}]^{2+}$	*T-II*	1.76	2.7	4.7	C_3-*IIIb*	1.40	0.0	0.0
	$[HgAg_{20}(L)_{12}]^{2+}$	*T-II*	1.57	1.1	2.3	C_3-*IIb*	1.58	0.0	0.0

Discussion

Assuming little energetic and bonding differences between structure-types *T*, C_3 and C_1, the major discriminant factor in the $[MAg_{20}(E_2PH_2)_{12}]^q$ structural choice is between types I, II and III, as stated in Table 3, which summarizes in a condensed way the data of Tables 2, S2 and S3. There are several factors that interplay in the preference between the three types of sites for M, the first one coming to mind being the size effect. Trends related to size effect are in fact not so obvious to apprehend, except that a small M atom (such as Zn) encapsulated within an Ag_{12} icosahedron is likely not to be very favorable. Another factor is electronegativity.

Table 3. M site occupation preference in the computed $[MAg_{20}(E_2PH_2)_{12}]^q$ species. Values in parentheses are Pauling electronegativities

Co (1.88) **E = S, Se:** I > III > II	**Ni** (1.91) **E = S, Se:** I > III > II	**Cu** (1.90) **E = S, Se:** III > I > II	**Zn** (1.65) **E = S, Se:** III > I > II
Rh (2.28) **E = S, Se:** I > III > II	**Pd** (2.20) **E = S, Se:** I > II ≈ III	**Ag** (1.93)	**Cd** (1.69) **E = S, Se:** II ≈ III > I
Ir (2.20) **E = S:** I > III > II **E = Se**: I > II ≈ III	**Pt** (2.28) **E = S:** I > II > III **E = Se:** I > II ≈ III	**Au** (2.54) **E = S, Se:** I > II > III	**Hg** (2.00) **E = S, Se:** II > I > III

From this strict point of view, starting from an homometallic $[Ag_{21}(E_2PH_2)_{12}]^+$ cluster, and substituting one Ag atom by a more electronegative atom will favor the more electron-rich site, thus type I (see the NAO charges in Table 1). Substituting Ag by a more electropositive atom will lead to the opposite choice, thus type III (see the NAO charges in Table 1). The preference for type III is also related to the ability for M, when in an oxidation state corresponding to the valence d^{10} configuration, to stabilize trigonal planar coordination. Au(I) or Hg(II), for example are more prone to di- rather tri-coordination. In any case, the likely most important parameter is the availability of the M valence d orbitals when encapsulated within the Ag_{13} icosahedron (structure-type I). Whereas the role played by the occupied valence d-type AOs of M is negligible in structure-types II and III, it can be different when structure-type I is considered. As recalled in the introduction, the *superatomic* electron configuration of the $[Ag_{21}(E_2PH_2)_{12}]^+$ nanoclusters is $1S^2\ 1P^6\ 1D^0$. The 1S, 1P and 1D *superatomic* orbitals are mainly combinations of the 4s(Ag) AOs (with some 4p(Ag) admixture). However, the "non-bonding" occupied valence d orbitals of the encapsulated M have the same symmetry as the vacant 1D orbitals, and can mix with them, resulting in a stabilizing effect.[35] This effect is weak in the case of M = Ag, but can be stronger when M has valence d-orbitals that are more diffuse and/or higher in energy. This is reflected by the NAO valence d populations of M (Table 4) computed for the *T-I* structure-types. When M = Au or belongs to groups 9 and 10 (and especially with their heavier elements), lower d populations are found, indicating stronger valence d(M) bonding involvement, thus more favored type I structures. The opposite effect occurs when M = Cu or belongs to group 12. Such an effect has already been described when isoelectronically substituting by Os the central Au atom in the 8-electron *superatom* $[Au_{13}(dppe)_5Cl_2]^{3+}$,[66] as well as in related doped Ag_{25} isoelectronic thiolato nanoclusters.[40]

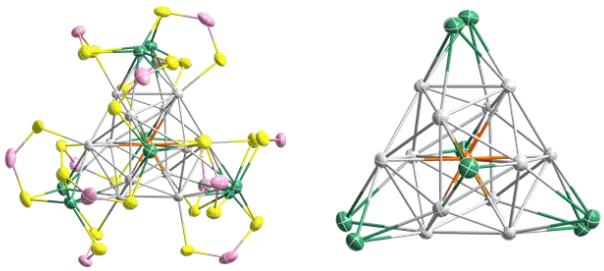

Figure 4. The *C_3-I* X-ray molecular structure of [{Pt@Ag_{20}}{$Se_2P(O^nPr)_2$}$_{12}$]. Left: Total structure with n-propoxy groups omitted for clarity. Right: Metal-framework. Color codes: orange, P; yellow, S; dark red, Pt; light blue, Ag_{ico}; pink, $Ag_{cap:}$ green.

Considering together both electronegativity and d-orbital effects allows understanding most of the results in Table 3. From these data it is also possible to reasonably predict the structure of polysubstituted species. For example, in the case of M = Au, the unique central site (type I) will be first occupied, then additional Au atoms will occupy icosahedron vertices (type II), as exemplified by the X-ray structure of [{Au@Au_2Ag_{18}}{$Se_2P(O^iPr)_2$}$_{12}$]$^+$.[47] The preference for outer capping positions for Cu (Type III) let to consider the theoretical limit number of 8 atoms in such positions. So far, up to 4 capping positions have been shown to be occupied by Cu in [{Ag@$Ag_{16}Cu_4$}{$S_2P(O^iPr)_2$}$_{12}$]$^+$ and [{Au@$Ag_{17}Cu_3$}{$S_2P(O^iPr)_2$}$_{12}$].[48] The isoelectronic substitution of two Ag atoms by two Ni or two group 9 metals is likely to involve the central site (type I) and one of the capping sites (type III). The group 12 situation is less clear, but in any case it is likely not to involve the central site (type I).

With respect to their optical properties, all the computed species have their lowest absorption energies associated with 1P →1D transitions and it is possible to anticipate their variations with respect to the nature of M by looking at their HOMO-LUMO gaps (Table 2). In the case of the most symmetrical type T-I structure type, the 1D level splits into two components (*t* and *e*) and the band of lowest energy is of 1P(*t*) →1D(*t*), nature, while the next one is of major 1P→1D(*e*) character. The simulated spectra of the E = Se species having type *T-I* structure type favored are shown in Figure 5a-c. They show typical blue-shift upon M descending a column and less variation within a given period. The experimental spectra of the [M@Ag_{20}{$S_2P(O^nPr)_2$}$_{12}$] (M = Ag, Au, Pt) clusters are reported in Figure 5c for comparison. Their λ_{max} values are 496, 472 and 470 nm (low energy band) and 414, 392 and 391 nm (high energy band) for M = Ag, Au, Pt, respectively. The corresponding computed values for the models [MAg_{20}{S_2PH_2}$_{12}$] (M = Ag, Au, Pt) are 474, 447, 445 nm (low energy band) and (395, 376 and 370 nm (high energy band), respectively (Figure 5c). Thus, with a small blue-shift of ~ 20 nm, the CAM-B3LYP-simulated spectra are in a very good agreement with their available experimental counterparts.

Table 4. Valence d NAO populations of M in the [M@$Ag_{20}(E_2PH_2)_{12}$]^q clusters of type *T-I*.

Co	9.43	**Ni**	9.73	**Cu**	9.97	**Zn**	10.0
Rh	9.32	**Pd**	9.70	**Ag**	9.91	**Cd**	9.98
Ir	9.37	**Pt**	9.75	**Au**	9.92	**Hg**	9.92

Conclusions

In summary, DFT calculations on 8-electron [M$Ag_{20}(E_2PH_2)_{12}$]^q (E = S, Se) silver-rich nanoclusters indicate that if M = Au or belongs to Groups 9 or 10, M clearly prefers occupying the central encapsulated site (Type I). If M = Cu,

the outer capping positions, *i.e.* Cu(I) (type III), is favored. All the known alloy species containing Au, Pt, Pd and/or Cu[41,43-48] follow our computed tends. These results are broadly consistent with those previously obtained by DFT calculations on 8-electron $[MAg_{24}(SR)_{18}]^q$ models that also contain a centered icosahedral core,[35] and with most of the known X-ray structures of such species.[67-71] Although no $[MAg_{20}(E_2PH_2)_{12}]^q$ alloy containing group 12 elements is known so far, our computed structures, HOMO-LUMO gaps, and bonding parameters suggest that such species should to be sufficiently stable for being isolated, with the preferred structure-type III, II/III and II for M = Zn, Cd and Hg, respectively. From the point of view of modulating optical properties, structure II, which impairs the *superatomic* core, would be particularly interesting to stabilize. Experimental attempts to synthesize such species are currently underway in our group.

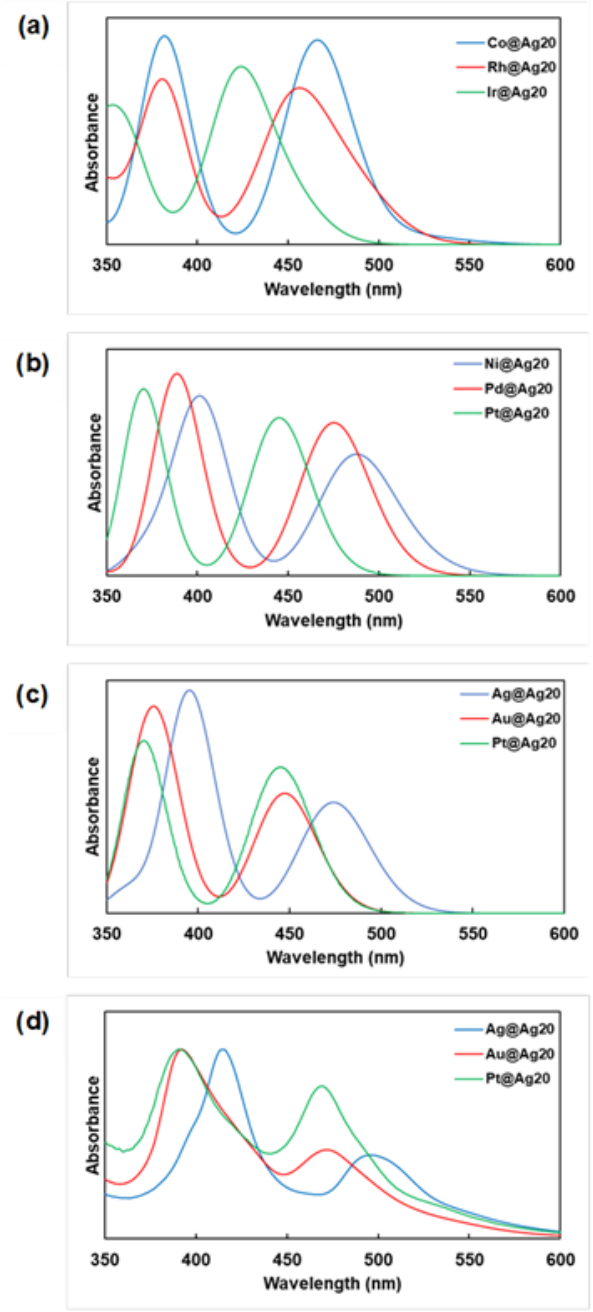

Figure 5. (a), (b) and (c): TD-DFT-simulated UV-vis spectra of the most stable isomers of the $[M@Ag_{20}(Se_2PH_2)_{12}]^q$ 8-electron species (*T-I* structure). (d) Experimental UV-vis spectra of $[M@Ag_{20}\{S_2P(O^nPr)_2\}_{12}]$ (M = Ag, Au, Pt) in 2-MeTHF solvent.

Conflicts of interest

There are no conflicts to declare.

Acknowledgements

This work was supported by the France-Taiwan ANR-MOST 2018 program (project Nanoalloys), the GENCI French national computer resource center (grant A0030807367) and the Ministry of Science and Technology of Taiwan (MOST 109-2113-M-259-008; 108-2923-M-259-001).

Notes and references

1 M. Walter, J. Akola, O. Lopez-Acevedo, P. D. Jadzinsky, G. Calero, C. J. Ackerson, R. L. Whetten, H. Gronbeck and H. Häkkinen, *Proc. Natl. Acad. Sci. U. S. A.*, 2008, **105**, 9157–9162.

2 H. Häkkinen, *Chem. Soc. Rev*., 2008, **37**, 1847–1859.

3 B. K. Teo, *J. Clust. Sci.*, 2014, **25**, 5–28.

4 R. Jin, C. Zeng, M. Zhou and Y. Chen, *Chem. Rev*., 2016, **116**, 10346–10413.
I. Chakraborty and T. Pradeep, *Chem. Rev*., 2017, **117**, 8208–8271.

5 G. Hu, Q. Tang, D. Lee, Z. Wu and D.-e. Jiang, *Chem. Mater.,* 2017, **29**, 4840–4847.

6 K. D. Weerawardene, H. Häkkinen and C. M. Aikens, *Annu. Rev. Phys. Chem.*, 2018, **69**, 205–229.

7 Q. Yao, T. Chen, X. Yuan and J. Xie, *Acc. Chem. Rev*., 2018, **51**, 1338–1348.

8 N. A. Sakthivel and A. Dass, *Acc. Chem. Rev*., 2018, **51**, 1774–1783.

9 Z. Lei, X.-K. Wan, S. F. Yuan, Z.-J. Guan and Q.-M. Wang, *Acc. Chem. Rev.*, 2018, **51**, 2465–2474.

10 T. Higaki, Q. Li, M. Zhou, S. Zhao, Y. Li, S. Li and R. Jin, *Acc. Chem. Rev.*, 2018, **51**, 2764–2773.

11 J. Yan, B. K. Teo and N. Zheng, *Acc. Chem. Rev*., 2018, **51**, 3084–3093.

12 S. Sharma, K. K. Chakrahari, J.-Y. Saillard and C. W. Liu, *Acc. Chem. Res.*, 2018, **51**, 2475–2483.

13 C. A. Smith, M. R. Narouz, P. A. Lummis, I. Singh, A. Nazemi, C. H. Li and M. C. Crudden, *Chem. Rev.*, 2019, **119**, 4986–5056.

14 Y. Du, H. Sheng, D. Astruc and M. Zhu, *Chem. Rev*., 2019, **120**, 526–622.

15 X. Kang and M. Zhu, *Chem. Soc. Rev*., 2019, **48**, 2422–2457.

16 T. Omoda, S. Takano and T. Tsukuda, *Small*, 2020, 2001439.

17 X. Kang, Y. Li, M. Zhu and R. Jin, *Chem. Soc. Rev*., 2020, **49**, 6443–6514.

18 H. Hirai, S. Ito, S. Takano, K. Koyasu and T. Tsukuda, *Chem. Sci.*, 2020, **11**, 12233–12248.

19 M. Kim, K. L. Dimuthu, M. Weerawardene, W. Choi, S. M. Han, J. Paik, Y. Kim, M.-G. Choi, C. M. Aikens and D. Lee, *Chem. Mater.*, 2020, **32**, 10216–10226.

20 K. Esma and T. Pradeep, *ACS Omega*, 2021, **6**, 1–16.

21 S. Takano and T. Tsukuda, *J. Am. Chem. Soc.*, 2021, **143**, 1683–1698.

22 F. Gam, J. Wei, S. Kahlal, J.-Y. Saillard and J.-F. Halet, *Struct. Bond.*, 2021, doi.org/10.1007/430_2021_81.

23 H. Yi, S. M. Han, S. Song, M. Kim, E. Sim and D. Lee, *Angew. Chem. Int. Ed.*, 2021, doi.org/10.1002/anie.202106311.

24 O. López-Estrada, E. Selenius, B. Zuniga-Gutierrez, S. Malola and H. Häkkinen, *J. Chem. Phys.*, 2021, **154**, 204303.

25 M. Walter and M. Moseler, *J. Phys. Chem. C*, 2009, **113**, 15834–15837.

26 D.-e. Jiang and S. Dai, *Inorg. Chem*., 2009, **48**, 2720–2722.

27 K. A. Kacprzak, L. Lehtovaara, J. Akola, O. Lopez-Acevedo and H. Häkkinen, *Phys. Chem. Chem. Phys.*, 2009, **11**, 7123–7129.

28 E. B. Guidez, V. Mäkinen, H. Häkkinen and C. M. Aikens, *J. Phys. Chem. C*, 2012, **116**, 20617–20624.
29 H. Qian, D.-e. Jiang, G. Li, C. Gayathri, A. Das, R. R. Gil and R. Jin, *J. Am. Chem. Soc.*, 2012, **134**, 16159–16162.
30 D. R. Kauffman, D. Alfonso, C. Matranga, H. Qian and R. Jin, *J. Phys. Chem. C*, 2013, **117**, 7914–7923.
31 T. Iwasa, K. Nobusada, A. Nakajima, *J. Phys. Chem. C*, 2013, **117**, 24586–24591.
32 L. Liao, S. Zhou, Y. Dai, L. Liu, C. Yao, C. Fu, J. Yang and Z. Wu, *J. Am. Chem. Soc.*, 2015, **137**, 9511–9514.
33 K. Kwak, Q. Tang, M. Kim, D.-e. Jiang and D. Lee, *J. Am. Chem. Soc.*, 2015, **137**, 10833–10840.
34 S. Wang, Y. Song, S. Jin, X. Liu, J. Zhang, Y. Pei, X. Meng, M. Chen, P. Li and M. Zhu, *J. Am. Chem. Soc.*, 2015, **137**, 4018–4021.
35 K. R. Krishnadas, A. Baksi, A. Ghosh, G. Natarajan and T. Pradeep, *ACS Nano*, 2017, **11**, 6015–6023.
36 F. Alkan, A. Muñoz-Castro and C. M. Aikens, *Nanoscale*, 2017, **9**, 15825–15834.
37 M. G. Taylor and G. Mpourmpakis, *J. Phys. Chem. Lett.*, 2018, **9**, 6773–6778.
38 F. Alkan, P. Pandeya and C. M. Aikens, *J. Phys. Chem. C*, 2019, **123**, 9516–9527.
39 W. Fei, S. Antonello, T. Dainese, A. Dolmella, M. Lahtinen, K. Rissanen, A. Venzo and F. Maran, *J. Am. Chem. Soc.* 2019, **141**, 16033–16045.
40 W.-T. Chang, P.-Y. Lee, J.-H. Liao, K. K. Chakrahari, S. Kahlal, Y.-C. Liu, M.-H. Chiang, J.-Y. Saillard and C. W. Liu, *Angew. Chem. Int. Ed.*, 2017, **56**, 10178–10182.
41 R. S. Dhayal, J.-H. Liao, Y.-C. Liu, M.-H. Chiang, S. Kahlal, J.-Y. Saillard and C. W. Liu, *Angew. Chem. Int. Ed.*, 2015, **54**, 3702–3706.
42 T.-H. Chiu, J.-H. Liao, F. Gam, I. Chantrenne, S. Kahlal, J.-Y. Saillard and C. W. Liu, *J. Am. Chem. Soc.*, 2019, **141**, 12957–12961.
43 T.-H. Chiu, J.-H. Liao, F. Gam, I. Chantrenne, S. Kahlal, J.-Y. Saillard and C. W. Liu, *Nanoscale*, 2021, **13**, 12143–12148.
44 B. S. Kumar, T.-H Chiu, Y.-C. Liu, M.-H. Chiang, F. Gam, I. Chantrenne, S. Kahlal, J.-Y. Saillard and C. W. Liu, *Nanoscale*, 2019, **11**, 14581–14586.
45 J.-H. Liao, S. Kahlal, Y.-C. Liu, M.-H. Chiang, J.-Y. Saillard, C. W. Liu, *J. Cluster Sci.*, 2018, **29**, 827–835.
46 W.-T. Chang, S. Sharma, J.-H. Liao, S. Kahlal, Y.-C. Liu, M.-H. Chiang, J.-Y. Saillard and C. W. Liu, *Chem. Eur. J.*, 2018, **24**, 14352–14357.
47 Y.-J. Zhong, J.-H. Liao, T.-H. Chiu, F. Gam, S. Kahlal, J.-Y. Saillard and C. W. Liu, *J. Chem. Phys.*, 2021, **155**, 034304.
48 S. N. Khanna and P. Jena, *Phys. Rev. Lett.*, 1992, **69**, 1664–1667.
49 S. N. Khanna and P. Jena, *Phys. Rev. B: Condens. Matter Mater. Phys.*, 1995, **51**, 13705–13716.
50 Gaussian 16, Revision A.03, M. J. Frisch, G. W. Trucks, H. B. Schlegel, G. E. Scuseria, M. A. Robb, J. R. Cheeseman, G. Scalmani, V. Barone, G. A. Petersson, H. Nakatsuji, X. Li, M. Caricato, A. V. Marenich, J. Bloino, B. G. Janesko, R. Gomperts, B. Mennucci, H. P. Hratchian, J. V. Ortiz, A. F. Izmaylov, J. L. Sonnenberg, D. Williams-Young, F. Ding, F. Lipparini, F. Egidi, J. Goings, B. Peng, A. Petrone, T. Henderson, D. Ranasinghe, V. G. Zakrzewski, J. Gao, N. Rega, G. Zheng, W. Liang, M. Hada, M. Ehara, K. Toyota, R. Fukuda, J. Hasegawa, M. Ishida, T. Nakajima, Y. Honda, O. Kitao, H. Nakai, T. Vreven, K. Throssell, J. A. Montgomery, Jr., J. E. Peralta, F. Ogliaro, M. J. Bearpark, J. J. Heyd, E. N. Brothers, K. N. Kudin, V. N. Staroverov, T. A. Keith, R. Kobayashi, J. Normand, K. Raghavachari, A. P. Rendell, J. C. Burant, S. S. Iyengar, J. Tomasi, M. Cossi, J. M. Millam, M. Klene, C. Adamo, R. Cammi, J. W. Ochterski, R. L. Martin, K. Morokuma, O. Farkas, J. B. Foresman and D. J. Fox, Gaussian, Inc., Wallingford CT, 2016.
51 Y.-R. Lin, P. V. V. N. Kishore, J.-H. Liao, S. Kahlal, Y.-C. Liu, M.-H. Chiang, J.-Y. Saillard and C. W. Liu, *Nanoscale*, 2018, **10**, 6855–6860.

A. D. Becke, *Phys. Rev. A*, 1988, **38**, 3098–3100.
52 J. P. Perdew, *Phys. Rev. B*, 1986, **33**, 8822–8824.
A. Schaefer, H. Horn and R. Ahlrichs, *J. Chem. Phys*., 1992, **97**, 2571–2577.
53 Schaefer, C. Huber and R. Ahlrichs, *J. Chem. Phys*., 1994, **100**, 5829–5835.
54 E. D. Glendening, J. K. Badenhoop, A. E. Reed, J. E. Carpenter, J. A. Bohmann, C. M. Morales, C. R. Landis and F. Weinhold, NBO 6.0, Theoretical Chemistry Institute, University of Wisconsin, Madison, WI, 2013, http://nbo6.chem.wisc.edu.
55 T. Yanai, D. Tew and N. Handy, *Chem. Phys. Lett*., 2004, **393**, 51–57.
56 GaussView, Version 6.1, R. Dennington, T. A. Keith, M. Millam, Semichem Inc., Shawnee Mission, KS, 2016.
57 SADABS, version 2014-11.0, Bruker Area Detector Absorption Corrections (Bruker AXS Inc., Madison, WI, 2014).
58 SAINT, included in G. Jogl, V4.043: Software for the CCD detector system (Bruker Analytical: Madison, WI, 1995).
59 G. M. Sheldrick, *Acta Cryst. A*, 2008, **64**, 112–122.
60 T. Gruene, H. W. Hahn, A. V. Luebben, F. Meilleur and G. M. Sheldrick, *J. Appl. Cryst*. 2014, **47**, 462–466.
61 SHELXTL, version 6.14. (Bruker AXS Inc., Madison, Wisconsin, USA, 2003).
62 Another C_1 structure, slightly different from that of Fig. 1 and not considered here, was identified in a complex co-crystal structure: J.-H. Liao, S. Kahlal, Y.-C. Liu, M.-H. Chiang, J.-Y. Saillard and C. W. Liu., *J. Clust. Sci.*, 2018, **29**, 827–835.
63 J. Wei, P. L. Rodriguez-Kessler, J.-F. Halet, S. Kahlal, J.-Y. Saillard and A. Muñoz-Castro, *Inorg. Chem.*, 2021, **60**, 8173–8180.
64 J. Yan, H. Su, H. Yang, S. Malola, S. Lin, H. Häkkinen and N. Zheng, *J. Am. Chem. Soc.*, 2015, **137**, 11880–11883.
65 M. S. Bootharaju, C. P. Joshi, M. R. Parida, O. F. Mohammed and O. M. Bakr, *Angew. Chem. Int. Ed.*, 2016, **55**, 922–926.
66 X. Liu, J. Yuan, C. Yao, J. Chen, L. Li, X. Bao, J. Yang and Z. Wu, *J. Phys. Chem. C*, 2017, **121**, 13848–13853.
67 L. He, Z. Gan, N. Xia, L. Liao, Z. Wu, *Angew. Chem. Int. Ed*., 2019, **58**, 9897–9901.
68 M. Kim, K. L. D. M. Weerawardene, W. Choi, S. M. Han, J. Paik, Y. Kim, M.-G. Choi, C. M. Aikens and D. Lee, *Chem. Mater.*, 2020, **32**, 10216–10226.

Table of Content

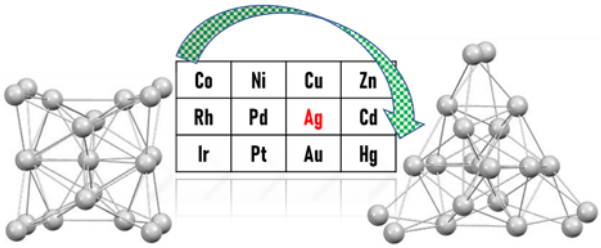

Doping $[Ag_{21}\{E_2P(OR)_2\}_{12}]^+$ (E = S, Se) nanoclusters